

## Inertial Effects on Fluid Flow through Disordered Porous Media

J. S. Andrade, Jr.,<sup>1,3</sup> U. M. S. Costa,<sup>1</sup> M. P. Almeida,<sup>1</sup> H. A. Makse,<sup>2</sup> and H. E. Stanley<sup>3</sup>

<sup>1</sup>*Departamento de Física, Universidade Federal do Ceará, 60451-970 Fortaleza, Ceará, Brazil*

<sup>2</sup>*Schlumberger-Doll Research, Old Quarry Road, Ridgefield, Connecticut 06877*

<sup>3</sup>*Center for Polymer Studies and Physics Department, Boston University, Boston, Massachusetts 02215*

(Received 16 October 1998; revised manuscript received 30 March 1999)

We investigate the origin of the deviations from the classical Darcy law by numerical simulation of the Navier-Stokes equations in two-dimensional disordered porous media. We apply the Forchheimer equation as a phenomenological model to correlate the variations of the friction factor for different porosities and flow conditions. At sufficiently high Reynolds numbers, when inertia becomes relevant, we observe a transition from linear to nonlinear behavior which is typical of experiments. We find that such a transition can be understood and statistically characterized in terms of the spatial distribution of kinetic energy in the system. [S0031-9007(99)09541-1]

PACS numbers: 47.55.Mh, 47.11.+j

A standard approach in the investigation of single-phase fluid flow in microscopically disordered and macroscopically homogeneous porous media is to characterize the system in terms of Darcy's law [1–3], which assumes that a *global* index, the permeability  $k$ , relates the average fluid velocity  $V$  through the pores with the pressure drop  $\Delta P$  measured across the system,

$$V = -\frac{k}{\mu} \frac{\Delta P}{L}. \quad (1)$$

Here  $L$  is the length of the sample in the flow direction and  $\mu$  is the viscosity of the fluid. However, in order to understand the interplay between porous structure and fluid flow, it is necessary to examine *local* aspects of the pore space morphology and relate them to the relevant mechanisms of momentum transfer (viscous and inertial forces). This has been accomplished in previous studies [4–10] where computational simulations based on a detailed description of the pore space have been quite successful in predicting permeability coefficients and validating well-known relations on real porous materials.

In spite of its great applicability, the concept of permeability as a global index for flow should be restricted to viscous flow conditions or, more precisely, to small values of the Reynolds number. Unlike the sudden transition from laminar to turbulent flow in pipes and channels where there is a critical Reynolds number value separating the two regimes, experimental studies on flow through porous media have shown that the passage from linear (Darcy's law) to nonlinear behavior is more likely to be gradual (see Dullien [1], and references therein). It has then been argued [1] and confirmed by numerical simulations [11,12] that the contribution of inertia to the flow in the pore space should also be examined in the framework of the laminar flow regime before assuming that fully developed turbulence effects are present and relevant to momentum transport. Here we show by direct simulation of the Navier-Stokes equations that the departure from Darcy's law in flow through high porosity percola-

tion structures ( $\epsilon > \epsilon_c$ , when  $\epsilon_c$  is the critical percolation porosity) and at sufficiently high Reynolds numbers can also be explained in terms of the inertial contribution to the *laminar* fluid flow through the void space. The calculations we perform do not apply for unstable or turbulent Reynolds conditions. We then demonstrate that it is possible to *statistically* characterize the transition from linear to nonlinear behavior in terms of the distribution of kinetic energy. This allows us to elucidate certain features of the fluid flow phenomenon in irregular geometries that have not been studied before.

Our model for the pore connectivity is based on the general picture of site percolation disorder. Square obstacles are randomly removed from a  $64 \times 64$  square lattice until a porous space with a prescribed void fraction  $\epsilon$  is generated. The mathematical description for the detailed fluid mechanics in the interstitial pore space is based on the assumptions that we have steady state flow in isothermal conditions and the fluid is continuum, Newtonian, and incompressible. Thus, the continuity and Navier-Stokes equations reduce to

$$\nabla \cdot \mathbf{u} = 0, \quad (2)$$

$$\rho \mathbf{u} \cdot \nabla \mathbf{u} = -\nabla p + \mu \nabla^2 \mathbf{u}, \quad (3)$$

where  $\rho$  is the density of the fluid and  $\mathbf{u}$  and  $p$  are the local velocity and pressure fields, respectively. We use the nonslip boundary condition at the whole of the solid-fluid interface. End effects of the flow field established inside the pore structure (particularly significant at high Reynolds conditions) are minimized by attaching an inlet and an outlet to two opposite faces. At the inlet a constant inflow velocity in the normal direction to the boundary is specified, whereas at the outlet the rate of velocity change is assumed to be zero (gradientless boundary condition). Instead of periodic boundary conditions, we close the remaining two faces of the system with two additional columns of obstacles. This insulating condition reproduces more closely the experimental setup usually

adopted with real rocks and permeameters. The Reynolds number is defined here as  $Re \equiv \rho V d_p / \mu$  where  $d_p$  is the grain diameter [13]. For a given realization of the pore geometry and a fixed  $Re$ , the local velocity and pressure fields in the fluid phase are numerically obtained through discretization (see [10] for numerical details) by means of the control volume finite-difference technique [14,15]. Finally, from the area-averaged pressures at the inlet and outlet positions, the overall pressure drop can be readily calculated.

The classical approach to macroscopically characterize the effect of inertia on flow through real porous media is to use the Forchheimer equation [1,2],

$$-\frac{\Delta P}{L} = \alpha \mu V + \beta \rho V^2. \quad (4)$$

The coefficient  $\alpha$  corresponds to the reciprocal permeability of the porous material and  $\beta$  is usually called the “inertial parameter.” Both  $\alpha$  and  $\beta$  should depend on the porosity  $\epsilon$  of the porous material. At sufficiently low velocities, Eq. (4) reduces to Darcy’s law, Eq. (1). The term  $\beta \rho V^2$  can be interpreted as a second order correction to account for the contribution of inertial forces in fluid flow. Equation (4) is not a purely empirical expression, since it can be derived by an appropriate average of the Navier-Stokes equation for one-dimensional, steady incompressible laminar flow of a Newtonian fluid in a rigid porous medium [1]. Rearranging (4) in the form,

$$f = \frac{1}{Re'} + 1, \quad (5)$$

where  $f \equiv -\Delta P / L \beta \rho V^2$  and  $Re' \equiv \beta \rho V / \alpha \mu$ , we obtain a *friction factor–Reynolds number* type of correlation which is presumably “universal.” Equation (5) has been extensively and successfully used to correlate experimental data from a large variety of porous materials and a broad range of flow conditions [1]. Certainly, a better representation for experimental data in the non-Darcy flow regime can be obtained with the addition to the Forchheimer equation of third order corrections in the velocity [2,11,12]. The theoretical basis for this type of correction term, however, is still controversial.

Figure 1 shows the results of our flow simulations in terms of the Forchheimer variables  $f$  and  $Re'$  for three different values of lattice porosity ( $\epsilon = 0.7, 0.8, \text{ and } 0.9$ ). After computing and averaging the overall pressure drops for all realizations at different values of  $\epsilon$  and  $Re$ , we fit the results with Eq. (4) to estimate the coefficients  $\alpha$  and  $\beta$  and calculate  $f$  and  $Re'$ . In agreement with real flow experiments, we observe a transition from linear (Darcy’s law) to nonlinear flow. Moreover, the point of departure from linear to nonlinear behavior in the range  $10^{-2} < Re' < 10^{-1}$  is consistent with previous experimental observations. However, in the region  $6.2 \times 10^{-2} < Re' < 1.8$ , the Forchheimer equation generally overestimates the computed values of the friction factor.

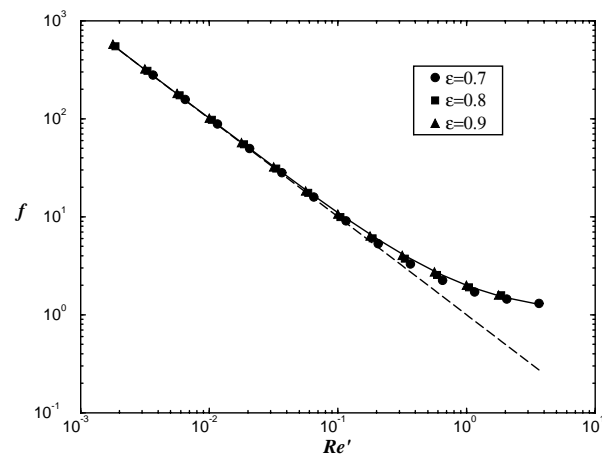


FIG. 1. Logarithmic plot showing the dependence of the generalized friction factor  $f$  on the modified Reynolds number  $Re'$ . The solid line is the best fit to the Forchheimer equation (4), while the dashed line is the best fit to Darcy’s law of the data at low  $Re'$ . Note that three pairs of  $\alpha$  and  $\beta$  parameters have been estimated for each of the three porosity values ( $\epsilon = 0.7, 0.8, \text{ and } 0.9$ ). These simulations have been performed with up to five lattice realizations. The error bars are smaller than the symbols.

In addition, for a fixed value of  $Re'$ , the variability in this transition region is sufficient to suggest a dependence of the type  $f = f(Re', \epsilon)$  [16].

The flow distribution in two-dimensional incompressible systems can be conveniently described in terms of the stream function  $\psi$  [17]. Figure 2a shows the contour plot of  $\psi$  for a typical realization of a highly porous void space ( $\epsilon = 0.9$ ) subjected to low Reynolds conditions,  $Re = 0.0156$ . In spite of the well-connected pathways available for flow at this large porosity value, the predominant viscous forces in the momentum transport through the complex void geometry generates well defined “preferential channels” of fluid flow. As shown in Fig. 2b, the situation is quite different at high  $Re$ , where the degree of channeling is clearly less intense than in Fig. 2a. In the case of Fig. 2b, due to the relevant contribution of inertial forces to the flow, the distribution of streamlines along the direction orthogonal to the main flux  $y$  becomes more homogeneous.

The channeling effect can be statistically quantified in terms of the spatial distribution of kinetic energy in the flowing system. In analogy with previous work on localization of vibrational modes in harmonic chains [18], we define a “participation” number  $\pi$ ,

$$\pi \equiv \left( n \sum_{i=1}^n q_i^2 \right)^{-1} \left( \frac{1}{n} \leq \pi \leq 1 \right), \quad (6)$$

where  $n$  is the total number of fluid cells in the numerical grid enclosing the physical pore space,  $q_i \equiv e_i / \sum_{j=1}^n e_j$ ,  $e_i \propto (u_i^2 + v_i^2)$  is the kinetic energy associated with each individual fluid cell, and  $u_i$  and  $v_i$  are the components of the velocity vector at cell  $i$  in the  $x$  and  $y$  directions,

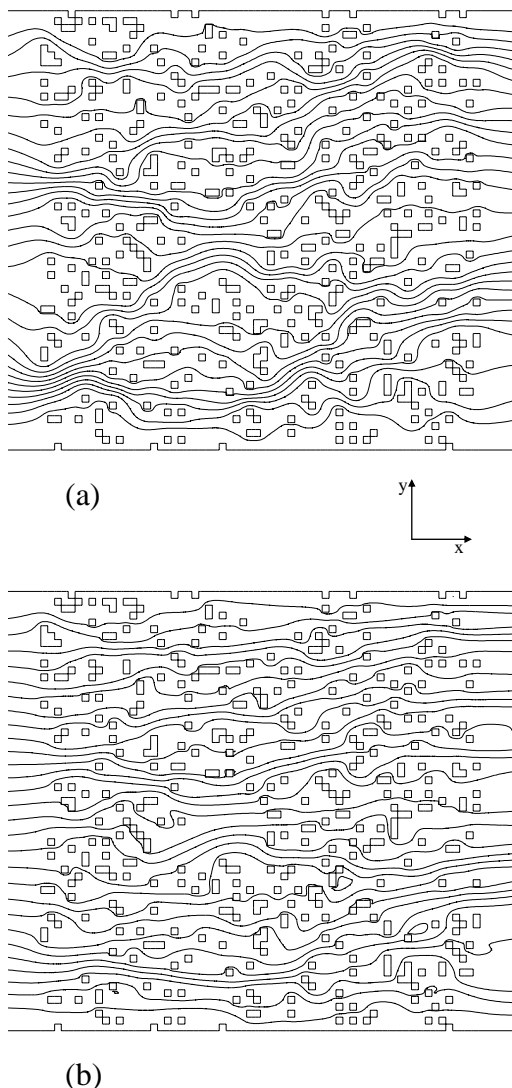


FIG. 2. (a) Contour plot of the stream function  $\psi$  for low Reynolds number conditions ( $Re = 0.0156$ ). (b) Same as in (a), but for a Reynolds number 1000 times larger ( $Re = 15.6$ ). In both plots, the values of  $\psi$  change by a constant increment between consecutive streamlines.

respectively. From the definition Eq. (6),  $\pi = 1$  indicates a limiting state of equal partition of kinetic energy ( $q_i = 1/n, \forall i$ ). On the other hand, a sufficiently large system ( $n \rightarrow \infty$ ) exhibiting strong channeling effects should correspond to a “localized” flow field,  $\pi \approx 0$  [19]. We calculate the function  $\pi$  for 10 pore space realizations generated with  $\epsilon = 0.9$  at different  $Re$ . Because of convergence difficulties and computational limitations on the resolution of the numerical grid, we restrict our calculations to  $Re \leq 15.6$ . As shown in Fig. 3, the participation number remains constant,  $\pi \approx 0.37$ , for low  $Re$  up to a transition point at about  $Re \approx 0.3$ . Above this point, the flow becomes gradually less localized ( $\pi$  increases) as  $Re$  increases. This transition reflects the onset of inertial effects in the flow, and the significant changes in  $\pi$  above

the transition point indicate the sensitivity of the system to these nonlinearities. The large error bars at low  $Re$  indicate that  $\pi$  is sensitive to structural disorder if the viscous forces are effectively generating preferential channels in the flow.

The difference between our results at low and high  $Re$  can be better understood if we remember that viscous effects extend a long way at low Reynolds conditions, so that distant boundaries may have a large effect on the streamlines. It is then interesting to visualize the distortions in the local velocity field when inertial forces become important compared to viscous forces. In Fig. 4 we show the profiles of the velocity magnitude at different positions along the main flow direction  $x$  in a typical realization of the porous media. At low  $Re$  (Fig. 4a), the fluctuations in the velocity field are essentially smooth in shape, with peaks that closely correspond to the variations in the local porosity. At high  $Re$  (Fig. 4b), the situation becomes quite different. Because of inertia, the effect on the flow field of the disorder in the local pore geometry tends to propagate further the fluctuations in the  $x$  direction. We can follow in Fig. 4b the changes in shape of the velocity magnitude at different  $x$  positions. If there is an available *straight* void space pathway for fluid flow, a peak generated at a smaller  $x$  can *persist* further right in the next profiles located at larger  $x$  values. As a consequence, the velocity profiles at large  $Re$  are more *rough* than those at low  $Re$ .

In summary, to characterize the influence of inertial forces on the flow of a single fluid in porous structures, we demonstrate that incipient deviations from Darcy’s law observed in several experiments can be modeled in the laminar regime of fluid flow, without including turbulence effects. The results of our simulations agree with numerous experimental data which display a gradual transition at high  $Re$  from linear to nonlinear flow in the pore space. Moreover, we show that this flow transition

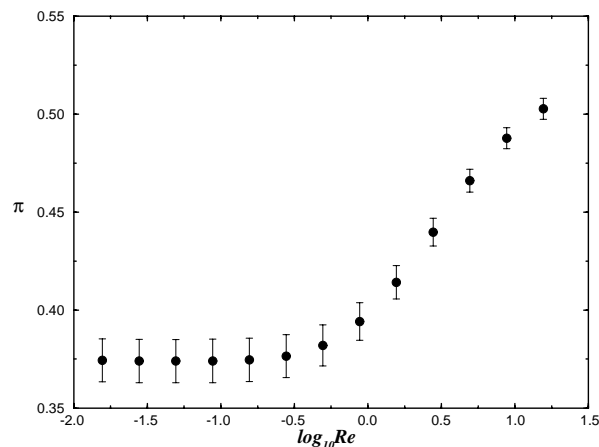


FIG. 3. Dependence of the participation number  $\pi$  on the Reynolds number  $Re$  ( $\epsilon = 0.9$ ). These simulations have been performed with ten lattice realizations.

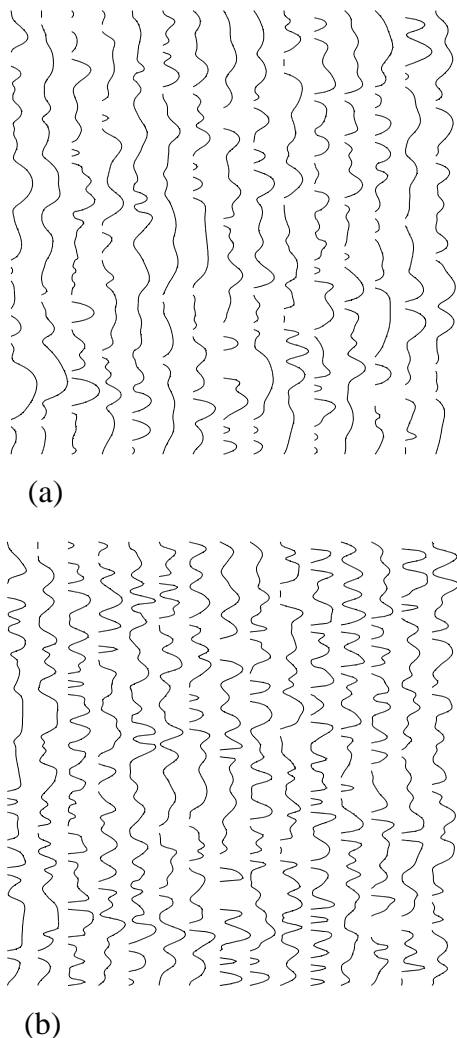


FIG. 4. (a) Profiles of the velocity magnitude at different positions in direction  $x$  for low Reynolds number conditions ( $Re = 0.0156$ ). The realization is the same as in Fig. 2, but the obstacles have been removed for better visualization. (b) Same as in (a), but for a Reynolds number 1000 times larger ( $Re = 15.6$ ). The velocity magnitudes in (a) and (b) have been normalized by the maximum value calculated for each system.

can be characterized in terms of the partition of kinetic energy in the fluid phase. Namely, the flow at low  $Re$  is more localized due to channeling effects than the flow at high  $Re$  conditions. Finally, our calculations with the Navier-Stokes equations indicate that the Forchheimer model should be valid for low  $Re$  and also for a limited range of high  $Re$  numbers, even when inertial nonlinearities can significantly affect the momentum transport at the pore scale. However, the magnitude of the deviations we find at the transition from Darcy to non-Darcy flow suggests a nonuniversal behavior of the friction factor  $f$  with the porosity  $\epsilon$  within this particular region.

We thank CNPq, FUNCAP, and NSF for support.

- [1] F. A. L. Dullien, *Porous Media—Fluid Transport and Pore Structure* (Academic, New York, 1979).
- [2] M. Sahimi, *Applications of Percolation Theory* (Taylor & Francis, London, 1994); *Flow and Transport in Porous Media and Fractured Rock* (VCH, Boston, 1995).
- [3] P. M. Adler, *Porous Media: Geometry and Transport* (Butterworth-Heinemann, Stoneham, MA, 1992).
- [4] D. H. Rothman, *Geophysics* **53**, 509 (1988); A. Cencieliere, C. Chang, E. Foti, D. H. Rothman, and S. Succi, *Phys. Fluids A* **2**, 2085 (1990).
- [5] S. Kostek, L. M. Schwartz, and D. L. Johnson, *Phys. Rev. B* **45**, 186 (1992).
- [6] N. Martys and E. J. Garboczi, *Phys. Rev. B* **46**, 6080 (1992).
- [7] L. M. Schwartz, N. Martys, D. P. Bentz, E. J. Garboczi, and S. Torquato, *Phys. Rev. E* **48**, 4584 (1993).
- [8] N. Martys, S. Torquato, and D. P. Bentz, *Phys. Rev. E* **50**, 403 (1994).
- [9] A. Koponen, M. Kataja, and J. Timonen, *Phys. Rev. E* **56**, 3319 (1997).
- [10] J. S. Andrade, Jr. *et al.*, *Phys. Rev. E* **51**, 5725 (1995); *Phys. Rev. Lett.* **79**, 3901 (1997).
- [11] D. A. Edwards, M. Shapiro, P. Bar-Yoseph, and M. Shapira, *Phys. Fluids* **2**, 45 (1990).
- [12] D. R. Koch and A. J. C. Ladd, *J. Fluid Mech.* **349**, 31 (1997).
- [13] The parameter  $d_p$  corresponds to the length of the side of the square plaquettes taken as obstacles for fluid flow in the two-dimensional lattice of size  $L$ . In all simulations  $L = 1$ , which makes  $d_p = 1/64$  in length units compatible with the density and viscosity units.
- [14] We discretize the governing balance equations within the pore space domain using square grid elements with length equal to  $d_p/4$ . In other words, while the physical system comprises  $64 \times 64$  elements (solid or fluid cells of size  $d_p$ ), the corresponding numerical mesh has  $256 \times 256$  discretization cells. We observe that this level of refinement generates satisfactory results when compared with numerical meshes of small resolution.
- [15] S. V. Patankar, *Numerical Heat Transfer and Fluid Flow* (Hemisphere, Washington, DC, 1980); The FLUENT (trademark of FLUENT Inc.) fluid dynamics analysis package has been used in this study.
- [16] S. L. Lee and J. H. Yang, *Int. J. Heat Mass Transf.* **40**, 3149 (1997).
- [17] The stream function  $\psi$  is defined for incompressible two-dimensional flows as  $u \equiv \partial\psi/\partial y$  and  $v \equiv -\partial\psi/\partial x$ .
- [18] S. Russ and B. Sapoval, *Phys. Rev. Lett.* **73**, 1570 (1994); B. Sapoval and S. Russ, *Nuovo Cimento Soc. Ital. Fis.* **16D**, 1103 (1994).
- [19] To provide a preliminary idea about the finite size effects on the participation function, we performed simulations with lattices of size  $96 \times 96$  ( $384 \times 384$  numerical elements) generated at a porosity  $\epsilon = 0.9$  and subjected to low  $Re$ . The results averaged over five realizations of the pore structure indicate that  $\pi = 0.32 \pm 0.01$ , a value which is substantially smaller ( $\approx 14\%$ ) than the value found for  $64 \times 64$  systems,  $\pi = 0.37 \pm 0.01$ .